J. Synchrotron Rad. (1997). **4**, 214–222

Application of Energy-Resolved Measurements to Laue Diffraction: Determination of Unit-Cell Parameters, Deconvolution of Harmonics and Assignment of Systematic Absences

Quentin S. Hanley,[a]† John W. Campbell[b] and M. Bonner Denton[a]*

[a]Department of Chemistry, University of Arizona, Tucson, AZ 85721, USA, and [b]CCLRC Daresbury Laboratory, Warrington WA4 4AD, UK. E-mail: mbdenton@ccit.arizona.edu

(*Received 28 October 1996; accepted 25 February 1997*)

The use of energy-resolved area detection of Laue diffraction patterns for the determination of unit-cell parameters and systematic absences is demonstrated. Seven different crystals having previously known unit cells were re-examined using Laue diffraction methods. These crystals included four different crystal systems including cubic, orthorhombic, tetragonal and monoclinic cells. The crystals had cell sizes ranging from 179.4 to 4588.3 Å^3. Comparison of known and re-determined cells showed good agreement (ratio of known to measured cells = 0.987 ± 0.18). A single procedure was suitable for all unit-cell determinations. The accuracy of the method is presently limited by the quality of the available energy measurements. Some of the crystals represent space groups containing systematic absences normally obscured by harmonic overlap when using the Laue method. These include absences due to 2_1 screw axes (h, k or $l = 2n + 1$) and cell centering ($h + k = 2n + 1$). All systematic absences were identified using a combination of multiple linear regression with either stepwise elimination or stepwise inclusion and an F test for assignment of systematic absence. The methods are discussed in detail and simulations are used to evaluate critical tolerances for future systems.

Keywords: unit-cell determination; Laue diffraction; screw axes; foil-mask spectrometers; harmonic deconvolution; systematic absences; energy-resolved measurements.

1. Introduction

Two problems and their consequences have generally limited the Laue method to systems which have been pre-examined using monochromatic methods. Using solely Laue data it is difficult to determine unit-cell dimensions accurately (Ravelli, Hezemans, Krabbendam & Kroon, 1996; Carr, Dodd & Harding, 1993; Carr, Cruickshank & Harding, 1992) and much information is hidden in the 10–20% of spots containing harmonic overlap (Cruickshank, Helliwell & Moffat, 1987). The multiple Laue spots contain information useful for the assignment of space groups (Amoros, Buerger & Canut de Amoros, 1975). Further, spots containing harmonic overlap come disproportionately from low-order reflections and other planes of special interest making the separation of the intensity components in the spot of particular concern (Hao, Harding & Campbell, 1995). Absence of these reflections from structure refinement systematically under-represents the low-frequency coefficients in the Fourier synthesis (Duke *et al.*, 1992; Bartunik, Bartsch & Qichen, 1992).

Early in the history of X-ray diffraction, methods were described whereby Laue photographs could be used to estimate unit-cell dimensions. These methods involved observing the low wavelength limit (λ_{min}) to the data and scaling the cell accordingly or assigning an energy to a spot and scaling the axial ratios to the energy of the spot. Bragg & Bragg (1924) described a method for single exposures. In their description the acceleration voltage on an X-ray tube was suggested as an estimate of λ_{min}. An alternative approach was described by Davey (1934). In this variation a series of exposures were taken as the acceleration voltage on an X-ray tube was decreased. Spot energy could be assigned by noting the voltage on the tube as the spot disappeared from the pattern.

A modern adaptation resembling the Braggs' method was described by Carr, Dodd & Harding (1993) and Carr, Cruickshank & Harding (1992), who define λ_{min} by inserting a metal foil into an incident 'white' beam from a synchrotron. The foil provides a sharp cutoff in the high-energy portion of the X-ray spectrum. This approach gave good results (within 0.5%) for monoclinic and orthorhombic cells having volumes in the range ~5 000–1 000 000 Å^3. The primary limitation of this method is that it works best with large unit cells. With small cells the diffraction pattern

† Current address: Max Planck Institute of Biophysical Chemistry, Department of Molecular Biology, Am Fassberg 11, D-37077 Göttingen, Germany.

is not well populated, making application of the method difficult.

An alternative, which more closely matches that described by Davey (1934), is to measure the energy of many spots in a Laue pattern. If such data are available the position and energies measured can be converted directly into positions in reciprocal space. For ideal data, plotting the reciprocal space coordinates results in a recognizable lattice. Cell determination can proceed regardless of orientation and is suitable for small unit cells. This approach is explored here.

Separation of multiply overlapped Laue diffraction spots has been the subject of several studies. The absorption of X-rays in film packs (Helliwell *et al.*, 1989) or in the foils of a ten-element foil-mask spectrometer (Hanley, Dunphy & Denton, 1996), direct methods (Hao, Campbell, Harding & Helliwell, 1993), mathematical deconvolution of different crystal orientations (Campbell & Hao, 1993), and a real-space density modification method (Hao, Harding & Campbell, 1995) have all been used to deconvolve the components in multiple Laue spots. With the exception of the foil-mask spectrometer, each of these methods has been subjected to crystallographic tests and has achieved considerable progress toward making low-frequency information available in structure refinement.

This paper describes the use of energy-resolved Laue data for the determination of unit-cell dimensions and separation of harmonically overlapped Laue spots. It consists of two approaches: (i) simulations are used to explore different limitations of the method and to define critical parameters for data acquisition, and (ii) data obtained from a foil-mask spectrometer system are used to measure unit cells and to separate harmonics. Further verification of the foil-mask spectrometer is included using the known cells.

2. Theory

2.1. *Unit-cell determination*

Energy-resolved Laue diffraction data give a direct view of the reciprocal lattice from which they came. The data can be converted directly to reciprocal space coordinates. The direction of any observed diffraction vector measured at a distance z from a crystal corresponds to the direction of a vector from the center of an Ewald sphere of radius $1/\lambda_{\rm meas}$. If $\lambda_{\rm meas}$ is known, the position of the point in the reciprocal lattice responsible for producing the diffraction may be calculated using

$$x' = x/[\lambda(x^2 + y^2 + z^2)^{1/2}],$$
$$y' = y/[\lambda(x^2 + y^2 + z^2)^{1/2}],$$
$$z' = z/[\lambda(x^2 + y^2 + z^2)^{1/2}] - 1/\lambda. \qquad (1)$$

These relationships are illustrated in Fig. 1.

With ideal data the observed spots form a readily indexable reciprocal lattice. In practice, the foil-mask spectrometer system produces imperfect energy data. Data sets may include reflections containing harmonic overlap, or spots for which the energy measurements are poor. The effect of such points may be minimized by selecting the best portions of the data set, but they cannot be completely eliminated *a priori*. For this reason the indexing method of Duisenberg (1992) was adopted. Briefly, the method consists of generating triplets created by the end points of three reciprocal space vectors corresponding to three reflections. If the reflections belong to a single reciprocal lattice, the normal to the triplet is a direct lattice vector. Reflection vectors are then projected onto the triplet normal and the line projection searches for the one-dimensional lattice with the shortest period giving a **t** vector. The three **t** vectors best fitting the data are used to determine a unit cell.

2.2. *Separation of harmonics*

Assignment of intensities to the components of multiply overlapped spots using a system of calibrated absorbers can be described by a multiple linear-regression model of the form

$$Y = \beta_1 x_1 + \beta_2 x_2 + \beta_3 x_3 + \ldots + \beta_n x_n + \varepsilon, \qquad (2)$$

where Y is the measured intensity, x_i is the known value of the transmission efficiency, β_i is the ith component of the multiply overlapped Laue spot, and ε is the error. This is a standard multiple linear-regression model except that the model is assumed to have zero intercept. This is due to the physical system in which no intensity is expected when all values of x_i are zero. A least-squares solution exists for this overdetermined system of equations. Using the matrix notation (Hanley, Dunphy & Denton, 1996) developed for the foil-mask spectrometer the intensity components are given by (3). In this equation the subscript t refers to the matrix transpose and the superscript -1 refers to the matrix inverse. **H** is the column vector containing each of the intensity components in the harmonic, T is the transmission

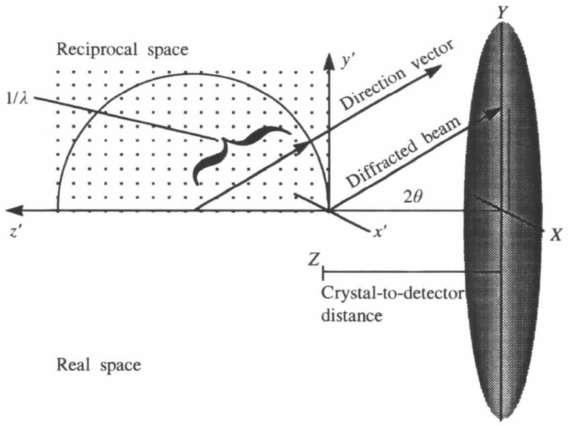

Figure 1
Illustration of the relationship between real and reciprocal space coordinates in a Laue diffraction pattern. Knowledge of the energy of the X-rays creating a spot in real-space coordinates (X, Y, Z) allows the reciprocal lattice coordinates (x, y, z) to be computed directly. The relationships shown in the picture are for illustration purposes and are slightly different than the convention used by the program *ERLAI*.

efficiency matrix, and $\mathbf{I}_m$ is the measured intensity through each of the foil masks.

$$\mathbf{H}_\lambda = (T^tT)^{-1}T^t\mathbf{I}_m. \quad (3)$$

The variance explained by the multiple linear-regression model is given by

$$ss_{reg} = \mathbf{H}_\lambda T^t\mathbf{I}_m. \quad (4)$$

The total variance is given by

$$ss_{tot} = \sum (I_i)^2. \quad (5)$$

The residual variance is given by

$$ss_{res} = ss_{tot} - ss_{reg}. \quad (6)$$

R^2 is the ratio of the variance explained by the multiple linear-regression model divided by the total variance. An adjusted R^2 value which takes into account the number of degrees of freedom in the model and the number of measurements made is given by

$$\text{Adj}\,R^2 = 1 - (1 - R^2)n/(n - k), \quad (7)$$

where n is the number of measurements (masks) and k is the number of intensity components in the harmonically overlapped spot. Statistically rigorous errors can be assigned to each intensity component in the model by first computing the mean squared residual,

$$ms_{res} = ss_{res}/(n - k). \quad (8)$$

The standard error of the ith intensity component in an overlapped spot can be computed from the mean squared residual,

$$se_i = [ms_{res}(T^tT)_{ii}^{-1}]^{1/2}. \quad (9)$$

The quantity $(T^tT)_{ii}^{-1}$ corresponds to the diagonal elements in the inverse matrix computed in (3). The significance of each intensity component is then tested using Student's t,

$$t_i = I_i/se_i. \quad (10)$$

If the value corresponds to a probability less than 0.025 the component is included, otherwise it is eliminated.

The value of ε in (2) is limited by three types of noise: detector noise, source flicker and Poisson noise. The Poisson, or shot, noise may be divided into components from the background and signal of interest. An ideal system, one with no detector noise, a perfectly stable X-ray source and negligible background, will be limited by the Poisson, or shot, noise of the detected X-rays. The critical property of Poisson noise is that the magnitude depends on the strength of the incident signal,

$$\sigma_I = I^{1/2}. \quad (11)$$

For this reason a component of a multiply overlapped spot having an intensity less than twice the standard deviation of the largest component should be assigned a value of zero.

2.3. *Assigning systematic absences*

Assigning systematic absences based on measurements of reflections in a monochromatic experiment is usually done using relationships between signal level and noise. A common procedure is to mark a reflection as absent if the intensity of the reflection is less than k times the noise.* This approach is statistically questionable since if k is set to two, reflections might be marked as 'systematically absent' which are 'statistically present' with 95% confidence. Although initial mis-assignments of space groups are encountered when using this approach, experience has shown such procedures to be useful.

Assigning an absence to a reflection in a multiply overlapped spot in a Laue pattern may proceed in a similar fashion. Considering reflections on an individual basis, the following criteria are proposed for assigning an absence when using a system of calibrated absorbers. A reflection is present if:

(*a*) it has a regression coefficient with a significance level of 97.5% or greater when using (2);

(*b*) it has a positive magnitude;

(*c*) it has a magnitude greater than twice the square root of the intensity of the largest overlapped reflection.

If the reflection does not meet these three criteria it is designated as absent. It should be noted that using these criteria may result in exclusion of some reflections that might be present and that all reflections present in a multiply overlapped spot are not equally weighted in the measurements of spot intensity. The wavelength normalization curve of the detection system inherently under-represents the reflections at some wavelengths. There is no way to correct for this prior to deconvolution of the harmonics using a system of calibrated absorbers.

Assigning a 'systematic absence' to a set of reflections in a multiply overlapped spot or spots is slightly more complicated. Here the example of a 2_1 screw axis is treated. This may be done by considering two models: one is designated a complete model, the other a reduced model.† The complete model is given by (2). The reduced model, (12), consists of (2) except that all the coefficients having odd-numbered coefficients have been removed.

$$Y = \beta_2x_2 + \beta_4x_4 + \ldots + \beta_{2n}x_{2n} + \varepsilon. \quad (12)$$

The hypothesis being tested is that of systematic absence (*e.g.* $\beta_1 = \beta_3 = \beta_5 = \ldots = \beta_{2n+1} = 0$). The F statistic‡ corresponding to this hypothesis, (13), may then be used to confirm a systematic absence when $F > F_{\nu^2}^{\nu^1}(\alpha)$,

$$F = [(ss_1 - ss_2)/(k - g)]/[ss_2/(n - k)], \quad (13)$$

where ss_1 is the sum of squared errors for the reduced model computed using (6), ss_2 is the sum of squared errors

* k here is a constant defining the desired significance level. Values of k vary somewhat depending on the researcher and the data set being confronted, but values of 1, 2 and 3 are common.

† This treatment is based on one given by Scheaffer & McClave (1982).

‡ The F test used here is related to the Hamilton R ratio tests. For a discussion of this relationship see Hamilton (1965).

for the complete model computed using (6), $k - g$ is the number of absent intensity components, k is the number of intensity components in the complete model, n is the total sample size, ν_1 is $k - g$, the number of degrees of freedom in the numerator of (13), ν_2 is $n - k$, the number of degrees of freedom in the denominator of (13), and α is the desired significance level. This F statistic tests whether the null hypothesis, that a systematic absence is present, may be rejected.

3. Experimental

3.1. *Data collection*

The foil-mask spectrometer system has been previously described (Hanley, Dunphy & Denton, 1996). Data were collected using an indirect CID camera system (Hanley, True & Denton, 1995), an Enraf–Nonius FR571 X-ray source equipped with a Cu rotating anode, and a CAD-4 goniometer. Images were processed using the image reduction and analysis facility (IRAF). Within IRAF, spot positions were entered manually, centered, and intensities integrated. The integrated intensities are used to compute measured values of transmission efficiency, T_m. This requires that a satisfactory measurement of I_0 be available for each spot for which energy determinations are made. Energies were computed as previously described and sorted using (14) as a figure of merit,

$$\mathrm{FOM} = \left\{ \left[\sum (T_e - T_m)^2 \right] / n \right\}^{1/2}, \qquad (14)$$

where FOM is the figure of merit, T_e is the calculated transmission efficiency at the energy measured, T_m is the measured transmission efficiency, and n is the number of masks used in the computation of energy. Only spots having measured energies with FOM < 0.05 were included in unit-cell parameter computations. The CID camera system crystal-to-detector distance and spatial distortions were calibrated using a sample of $MoOCl_4PC_{24}H_{20}$.

Six crystals were selected for study: NaCl, KCl, $C_{19}H_{28}O_2$, $MoOS_4N_4C_{28}H_{40}$, $C_{19}H_{31}MoBN_6O_3$ and $MoOCl_4PC_{24}H_{20}$. Crystals were mounted in a random orientation.

3.2. *Computations*

Several programs were written to evaluate the system and perform computations on the collected data. These programs are *ERLAI*, *EMATCH*, *EINDEX*, *ESIMUL*, *ESEP* and *EAN*. *ERLAI* is used for the determination of unit-cell parameters and orientation using a set of energy-resolved measurements. *EMATCH* rescales unit cells determined by *ERLAI* following refinement using *LAUEGEN* and reduction by *TRACER*.* *EINDEX* assigns indices, multiplicity and harmonic increments to spots in a Laue diffraction pattern. *ESIMUL* generates a simulated energy-resolved data set given a Laue data module file. *ESEP* separates harmonics and tests for 2_1 (and related systematic absences) and 4_1 screw axes. *EAN* adds Gaussian noise to a set of energy-resolved Laue data for simulation purposes.

The method of Duisenberg (1992) was adopted and coded in the program *ERLAI*. The program first converts the spot positions and energies into reciprocal lattice coordinates. The auto-indexing procedure is then carried out. All triplets (the end points of three reflection vectors) are generated for the selected input reflections and the origin reflection. The normals to such triplets define direct-lattice vector directions if the three reflections belong to the same reciprocal lattice. Taking each triplet in turn, all the selected reflections are projected onto it and the line projection is searched for the one-dimensional lattice with the shortest period above a minimum value (defined by twice a user-entered variable *CELL MAX*) that fits the maximum number of the reflections within a requested tolerance (*FIT LEVEL* and *FIT INDEX*) giving a **t** vector which is stored. In *ERLAI*, all triplets are examined from the start rather than taking a random selection initially as done by Duisenberg. The **t** vectors list is sorted in descending order of *NFIT* (the number of fitting reflections) and the determined reciprocal distance vector **d***. The first vector in the sorted list is chosen to be the first direct-lattice vector. The list is then searched to find the next vector which is at least a user-defined minimum angle (default 30°) from the first selected vector. This defines the second direct-lattice vector. The search continues to find a third vector which is at least a user-defined minimum angle (default 30°) from the first two vectors. The three selected **t** vectors are then refined as described by Clegg (1984). The reflections which index well using the three vectors are found and if there are a sufficient number of these (*e.g.* at least half of the starting set of reflections) then the three selected **t** vectors are re-refined using only the fitting reflections. If the vectors form a left-handed set then they are converted into a right-handed set. During processing with *ERLAI*, an estimated maximum cell length was obtained by an iterative procedure. Typically, the largest number of spots fitting the computed cell was observed when *CELL MAX* is set to half of the longest unit-cell dimension. The half value reflects the computation algorithm used by *ERLAI*. In the region of rapid increase a series of estimated values were entered in 0.5 Å increments until the lowest maximum cell length with the largest number of fitting spots was selected for cell determination. The cell and crystal orientation are then determined and output to a file in a suitable format for input to the *LAUEGEN* program.

The programs *EMATCH*, *EINDEX* and *ESIMUL* make use of the Laue data module routines (Campbell, Clifton, Harding & Hao, 1995) from the Daresbury Laboratory *Laue Software Suite*. *EMATCH* predicts the reflection positions on an image and their energies given the current crystal and orientation parameters. For each observed reflection the program finds the predicted reflection which is closest to the observed position. It is treated as a match if the

* The version of *TRACER* used here is part of the *MolEN* analysis package supplied by Enraf–Nonius, Delft, The Netherlands.

distance between the observed and predicted position is less than a user-defined number of rasters (default = 2) and the fractional wavelength difference is less than another user-defined value (default 20%). The user may choose to include spots believed to be multiples if desired. Using the matching spots a least-squares calculation determines the scaling factor to apply to the cell to give the best match between the predicted and experimentally determined energies. Details of the spots found and matched are listed and the rescaled cell values are output. *EINDEX* works in a similar fashion except that all the data in the list, rather than only those with low FOMs, are processed. In assigning a match only the distance between the predicted and observed position is used. *ESIMUL* generates the position and energy of spots in a Laue pattern based on an Laue data module file. The first 249 of these are written to a file in *ERLAI* input format.

The program *ESEP* is an adaptation of the constrained multiple linear-regression procedures outlined in §§2.2 and 2.3. The matrix manipulation was performed using published algorithms (Embree & Kimble, 1991). *F* and *t* tests performed by the program are based on published algorithms (Vetterling, Teukolsky, Press & Flannery, 1988). The program constructs the *T* matrix using the data produced by *EINDEX* for the number, type and increment of the harmonics. The regression performed by *ESEP* is forced to include the origin and negative coefficients are rejected. When the predicted number of harmonics is less than or equal to four, a backward elimination procedure is used to eliminate components with *P* values greater than 0.025. When the predicted number of components exceeds four, a forward inclusion procedure is used to iteratively select components whose coefficients have *P* values less than 0.025. The program was verified against the *SPSS* program using data from selected spots.

The program *EAN* was used to validate *ERLAI*. *EAN* operates on files in *ERLAI* input format and adds user-specified amounts of Gaussian noise to the *xy* positions or energies contained in the file. *EAN* is based on a published random-number generator (Vetterling, Teukolsky, Press & Flannery, 1988).

3.3. *Data analysis*

The procedure for obtaining unit cells from the measured energies and positions consisted of five steps. First, the positions and energies were measured. Second, the measured positions and energies were submitted to the program *ERLAI* to obtain cell dimensions and orientation matrices. Third, the cell dimensions and orientation matrices were entered into *LAUEGEN* and both sets of parameters were refined. Fourth, the refined unit cell was submitted to *TRACER* to obtain a reduced cell. If necessary, the third and fourth steps were repeated until a good correspondence between the Laue pattern and the predicted pattern was obtained. Finally, predicted and observed energies were compared using the program *EMATCH* to ascertain whether the final cell needed rescaling. This last step is necessary because the position of spots is unaffected by rescaling a unit cell by a constant factor. If successive refinements and cell reduction are performed, the cell axis lengths begin to lose fidelity to the original data. Rescaling the cell following refinements and cell reduction guards against this and against the possibility of spurious cell-axis doubling during data reduction. Once a rescaled unit cell is found, the energy-resolved data list is indexed using *EINDEX* and separation of harmonics proceeds using *ESEP*.

Simulated data were treated using a slightly different procedure. When image data were not available, simulations 1 and 2, the output from *ERLAI* was submitted directly to *TRACER*. Simulation 3 was refined against real Laue data.

Table 1
Detector parameters for the CID system.

Parameter	Value
Crystal-to-detector distance	77.57 mm
X center position	234 rasters
Y center position	264 rasters
X center offset	0.052 mm
Y center offset	0.051 mm
Detector twist	4.761 (× 0.01°)
Detector tilt	22.748 (× 0.01°)
Detector bulge	−106.195 (× 0.01°)

4. Results

4.1. *Calibrations*

A sample of the $MoOCl_4PC_{24}H_{20}$ crystal was placed into the beam of the instrument and a standard Laue photograph was taken. The crystal orientation was found using *LAUEGEN* and the known cell parameters. A total of 227 spots were used, refining to a final r.m.s. of 0.093 mm. The resulting parameters for the CID camera system are given in Table 1.

All energy data for all crystals meeting the criteria for inclusion in unit-cell computations are plotted in Fig. 2 against the predicted energy based on orientations found

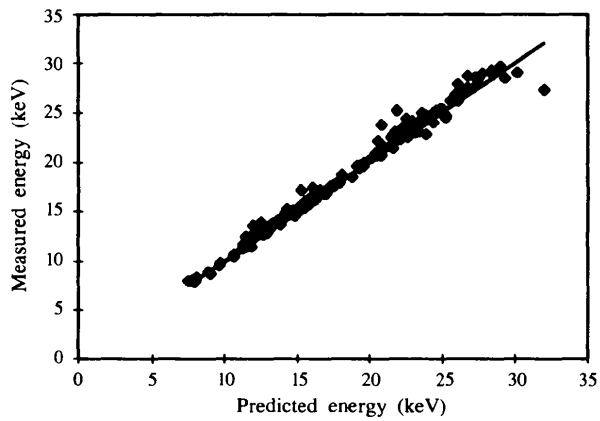

Figure 2
Correspondence between predicted and measured energies for the spots used for the determination of unit cells. The line in the figure is for ideal 1:1 correspondence.

Table 2
Simulation results.

Simulation No.	Initial parameters (Å, °)	Parameters obtained with 0% added noise (Å, °)	Parameters obtained with 1% added noise (Å, °)	Parameters obtained with 2% added noise (Å, °)	Parameters obtained with 3% added noise (Å, °)
1 – Cubic	a = 6.00	a = 6.00	a = 5.99	a = 6.02	a = 5.95
2 – Triclinic	a = 10.00	a = 10.00	a = 10.07		
	b = 27.11	b = 27.11	b = 26.30		
	c = 9.00	c = 9.00	c = 9.12		
	α = 98.27	α = 98.26	α = 98.79		
	β = 92.00	β = 92.00	β = 90.13		
	γ = 85.71	γ = 85.70	γ = 87.19		
3 – Monoclinic	a = 30.37	a = 30.37	a = 29.20*	a = 30.66	a = 30.57
	b = 8.37	b = 8.37	b = 8.45	b = 8.42	b = 8.43
	c = 19.65	c = 19.65	c = 19.53	c = 19.80	c = 19.79
	β = 113.28	β = 113.2	β = 108.77	β = 113.41	β = 113.42

* No refinement in *LAUEGEN* was used for this determination.

using the known cell parameters. Of the 783 spots measured in the Laue patterns, 207 (26.4%) met the criteria for inclusion. Fig. 2 includes data in which multiples were predicted to be present. From this data it appears that applying the inclusion criteria selects spots that are either singles or multiples in which only one harmonic dominates.

4.1.1. *Unit-cell determination – simulations.* Table 2 presents three simulations. Simulation 1 consisted of a cubic system with a 6 Å unit cell with all mis-setting angles set to zero. Simulation 2 consisted of a triclinic system viewed in a random orientation. Simulation 3 was an idealized case corresponding to $C_{19}H_{31}MoBN_6O_3$. The simulation was run using the orientation of the known cell, allowing refinement in *LAUEGEN*.

In all cases a combination of *ERLAI* and *TRACER* found the cell parameters of the simulated pattern without subsequent refinement in *LAUEGEN*. When 1% random noise was added to the idealized data a cell resembling the original cell was obtained. To obtain the cells reported after addition of 1% noise in Table 2 sometimes required increasing the fit-level parameters and the value of *DEL* used in *TRACER*. The agreement between the parameters used in the simulations and those recovered was degraded somewhat with the lower symmetry cells relative to the cubic cells.

Without refinement in *LAUEGEN* it was difficult to recover the original cells when the noise level reached 2%. With refinement, agreement within 1% of the original parameters was readily obtained, even after addition of 3% noise.

4.1.2. *Separation of harmonics – simulations.* Three simulations of a harmonic consisting of four Poisson intensity components were performed. Initially, the intensity components are 1×10^2, 1×10^3, 1×10^4 and 1×10^5, having standard deviations of 10, 31.6, 100 and 316, respectively. The intensity of the spots is then modeled as each intensity component grows by an order of magnitude. This corresponds to the case of increasing the length of exposure by factors of ten. In each simulation the intensity components are summed after attenuation by a T matrix to obtain **I**. In the first simulation only two harmonics could be separated. As the magnitude of the intensity components increases, the number of harmonics which could be separated and the significance associated with those components also increases. As the intensity of the **I** vector increases, the ability to separate the intensity components in the spots also increases. When insufficient signal is present the weaker components become lost in the noise from those of high intensity.

4.1.3. *Unit-cell determinations – real data.* A total of six crystals were examined. Each of these crystals have been previously characterized using monochromatic methods. A summary of each crystal is presented in Table 3.

The Laue pattern from NaCl had 29 spots. Of these, ten spots had FOMs ≤ 0.05 and were submitted to the program *ERLAI*. The pattern from KCl had 21 spots. Twelve of these had FOMs < 0.05. Three orientations of the crystal of $C_{19}H_{28}O_2$ were viewed. Each orientation was submitted to energy analysis. Orientation 1 ($0k0$) had 102 spots. Of these, 34 had FOMs < 0.05, and 50 were harmonics. Orientation 2 ($h00$) had 109 spots with 20 having FOMs < 0.05, and 50 were harmonics. Orientation 3 ($00l$) had 91 spots of which ten had FOMs ≤ 0.05, and 48 were harmonics. A cell could not be refined for orientation 3. Examination of the ten spots meeting inclusion criteria showed that only one was a true monochromatic reflection; the remainder contained harmonic overlap. The values in Table 3 are for orientations 1 and 2. The pattern from $MoOS_4N_4C_{28}H_{40}$ had 121 spots. 26 had FOMs < 0.05, and 39 were harmonics. The pattern for $C_{19}H_{31}MoBN_6O_3$ had 122 spots with 51 having FOMs < 0.05, and 39 were harmonics. The pattern from $MoOCl_4PC_{24}H_{20}$ had 188 spots of which 44 had FOMs < 0.05, and 38 were harmonics.

4.1.4. *Separation of harmonics.* The NaCl and KCl data sets contained no spots with harmonic overlap and were not analyzed further. Of the remaining data sets, 260 spots contained harmonic overlap. The number of predicted spots contained in these harmonics ranged from 2 to 12. The maximum number of intensity components into which any given spot was separated was four.

4.1.5. *Assignment of systematic absences.* Although the harmonics containing information for assigning screw

Table 3
Summary data for cells used in this study.

Compound	Crystal system	Space group	Known cell parameters (Å, °)	Measured cell parameters (Å, °)		Measured to known cell axes
NaCl*	Cubic	$Fm3m$	a = 5.6402	a = 5.60 ± 0.09		0.993
KCl†	Cubic	$Fm3m$	a = 6.2929 (1)	a = 6.16 ± 0.10‡		0.979
$C_{19}H_{28}O_2$§	Orthorhombic	$P2_12_12_1$	a = 11.333 (3)	a = 11.30 ± 0.23	a = 11.62 ± 0.30	1.01
			b = 12.813 (4)	b = 12.72 ± 0.25	b = 12.79 ± 0.33	0.995
			c = 11.290 (2)	c = 11.22 ± 0.22	c = 11.38 ± 0.30	1.00
$MoOS_4N_4C_{28}H_{40}$¶	Monoclinic	$P2_1/n$	a = 8.911 (3)	a = 8.87 ± 0.15		0.995
			b = 10.211 (6)	b = 10.16 ± 0.17		0.995
			c = 15.414 (1)	c = 15.38 ± 0.26		0.997
			β = 103.42 (3)	β = 103.58		
$MoOCl_4PC_{24}H_{20}$	Tetragonal	$P4/n$	a = 12.7379 (4)	a = 12.11 ± 0.43		0.951
			b = 12.7379 (7)	b = 12.11 ± 0.43		
			c = 7.6871 (3)	c = 7.31 ± 0.26		0.951
$C_{19}H_{31}MoBN_6O_3$**	Monoclinic	$C2/c$	a = 30.365 (4)	a = 30.1 ± 1.0		0.991
			b = 8.373 (1)	b = 8.29 ± 0.30		0.990
			c = 19.646 (2)	c = 19.50 ± 0.70		0.992
			β = 113.28 (1)	β = 113.25		
						Mean = 0.988
						Standard deviation = 0.018

* Data from Donnay & Ondik (1972), error assumed to be ±1 in final decimal place. † Data from Donnay & Ondik (1972). ‡ The weak spots in the KCl pattern were not observed in the Laue patterns. The cell was determined as primitive cubic with a = 3.08 Å. This has been doubled and reported in the table. § Data from Bruck (1997). ¶ Data from Bruck (1996). ** Data from Xiao *et al.* (1995).

Table 4
Assignment of systematic absences.

Compound	Type of symmetry	Reflection condition	Range of harmonics	Harmonics found	Harmonic type	Systematic absence found*		Correct assignment ?
						$2n + 1$	$4n + 1$	
$C_{19}H_{31}MoBN_6O_3$	Centering	$h + k = 2n$	2–4	2, 4	$(0,\bar{1},3)$	Yes	No	Yes
$C_{19}H_{31}MoBN_6O_3$	Screw	$l = 2n$	3–14	4, 8, 10	(0,0,1)	Yes†	No†	Yes
$C_{19}H_{31}MoBN_6O_3$	Centering	$h + k = 2n$	2–8	2, 6, 8	$(1,0,\bar{2})$	Yes	No	Yes
$C_{19}H_{31}MoBN_6O_3$	Centering	$h + k = 2n$	2–4	2	$(0,\bar{1},0)$	Yes	No	Yes
	Screw	$k = 2n$						
$C_{19}H_{28}O_2$ orientation 1	Screw	$k = 2n$	1–6	2, 4	$(0,\bar{1},0)$	Yes	No	Yes
$C_{19}H_{28}O_2$ orientation 1	Screw	$l = 2n$	2–10	4, 6	$(0,0,\bar{1})$	Yes	No	Yes
$C_{19}H_{28}O_2$ orientation 2	Screw	$l = 2n$	1–6	2, 4	(0,0,1)	Yes	No	Yes
$C_{19}H_{28}O_2$ orientation 3	Screw	$k = 2n$	1–7	2, 4	(0,1,0)	Yes	No	Yes
$MoOCl_4PC_{24}H_{20}$	None	None	2–7	3, 4	(0,0,1)	No	No	Yes

* Systematic absence was assigned if either the F test or the stepwise regression method revealed an absence of the type indicated. † F test for this set of harmonics could not be made. Number of coefficients exceeds available data.

axes were of most interest, only a very small number of spots of this type were observed. As a result, spots predicted to have systematic absences due to unit-cell centering were also examined. These results are presented in Table 4.

5. Discussion

5.1. *Simulations – unit-cell determination*

The simulations indicate that the determination of unit-cell parameters using energy-resolved data is applicable to a wide range of cell sizes and types. It allows all three axes to be determined in any orientation. The previously described methods (Carr, Dodd & Harding, 1993; Carr, Cruickshank & Harding, 1992) fail under some rare conditions. With the exception that the energy measurements must be of sufficient quality, the unit-cell determination methods described here are general. The simulations indicate that the tolerances required for the energy-resolved method are relatively loose. A 1% random error in energy measurements is easily tolerated and does not require refinement. If a refinement step is introduced, higher noise in the data may be present. These simulations indicate that a system capable of making energy-resolved measurements with less than 1% error should be suitable for most applications. More can be tolerated, but this represents a good design goal, regardless of the method by which the measurements are made.

The results of the simulation of non-random errors such as inaccurate determination of the crystal-to-detector distance or the xy position of spots indicate that these sorts of errors propagate almost linearly into inaccuracies in cell parameters. Consideration of equation (1) suggests why this occurs. If there is an inaccuracy in the determination of the square-root term in the denominator, it will result in an error in the reciprocal space position of the spot position. The exact magnitude of the inaccuracy depends on the relative magnitudes in the errors of the measurements of the X, Y and Z coordinates. Under special conditions, such as the

case where X, Y and Z are each off by a factor of two, the inaccuracies will cancel out.

5.2. *Simulations – harmonic separation*

The separation of the intensity components in a harmonically overlapped spot is limited by Poisson noise in the collected X-ray photons. The simulated harmonic separation illustrates that while a limitation exists, separation of harmonics is favored by high beam intensity. Like the energy measurements from a foil-mask spectrometer system (Hanley, Dunphy & Denton, 1996), the ability to separate harmonics improves with the total number of X-ray photons measured. The theoretical limitation is imposed once the intensity level is set.

As noted in §2.2 the error ε in the multiple linear-regression model also may contain contributions from detector dark-current noise, read noise and source $1/f$ (flicker) noise. Read noise in the measurement of X-rays varies depending on the system of measurement used. Use of photographic film can result in a large amount of read noise during digitization of the image. In this context it is interesting to compare the *UNSCRAM* procedure using stacked film (Helliwell *et al.*, 1989) with the foil-mask spectrometer system. Film will have greater uncertainty associated with the digitization of the image; however, a unique feature of the *UNSCRAM* approach is that the images are coincident in time, effectively eliminating source flicker noise. In contrast, the foil-mask spectrometer collects a series of images which are separated in time, making it sensitive to source instability during data collection. In environments where the X-ray source is not stable, corrections may be necessary. If it were possible to construct an image plate which, like film, was semi-transparent to X-rays and could be stacked, the *UNSCRAM* approach could become a method of choice for both energy determination and harmonic separation. It would also have the advantage of simultaneous acquisition of the multiple required images and, unlike film, could be calibrated once and reused repeatedly. A demonstration of the stacking of two image plates to record synchrotron protein crystal Laue patterns has been made by Helliwell (1991) in experimental trials at CHESS.

5.3. *Real data sets – unit-cell determination*

Analysis of the real data sets indicates that the foil-mask spectrometer gives energies that are suitable for unit-cell determination. In all cases moderate agreement with the known cells was obtained while requiring a minimum of operator intervention. A single procedure was suitable for all data sets suggesting that many steps could be automated. The combination of the programs *ERLAI*, *LAUEGEN* and *EMATCH* analyze the data from energy-resolved measurements of Laue patterns efficiently. The cells obtained using these programs fit the data almost as well or better than the known cells. This indicates that the measurement of cell parameters using this method is presently limited by the quality of the energy measurements. This conclusion is corroborated by the facility with which *ERLAI* was able to obtain cells using simulated data with low noise.

In comparison with previous work with Laue methods the energy-resolved measurements result in unit-cell dimensions of similar quality. The demonstration on small unit cells provides a complement to previously described methods (Carr, Dodd & Harding, 1993; Carr, Cruickshank & Harding, 1992). In addition, the previously described methods, which are based on the use of the gnomonic projection, can be difficult to carry out in practice. The required triangles and zone lines are often not easily identifiable from the experimentally determined gnomonic projections. Using either method it is clear that measurements obtained using Laue methods are of a lower quality than those made with monochromatic methods. However, another order of magnitude increase in the quality of the energy measurements may be possible in the near future and the present level of accuracy is certainly within the range of utility.

Additionally, this method may be a useful complement to previously described studies of very small crystals (Kariuki & Harding, 1995). The dimensions of the alkali halide crystals used here are in the range of many crystalline minerals. A single orientation was sufficient for the determination of the cell dimensions. Moreover, laboratory-scale instrumentation was sufficient for the present work.

5.4. *Real data – harmonic separation*

The use of the foil-mask spectrometer allows for identification of the most important intensity components in a harmonically overlapped spot. Careful attention to the residual variance after extracting the most significant components allows an upper bound to be placed on the magnitude of the harmonics which are not significantly present. For example, if the significant components explain 99.9% of the variance, all remaining components combined can account for no more that 0.1%. This is of particular importance in light of the systematic loss of low-frequency components in refinements which do not use data from harmonically overlapped spots. Using the foil-mask spectrometer data, at least the most important of these will be identified.

It is also of interest that in the data sets collected and analyzed here it was usually found that the number of harmonics predicted by reciprocal space geometry alone exceeded the number separated. Usually, one or two intensity components dominate. Some of this is due to the theoretical limitation discussed previously. It will never be possible to separate reliably harmonics in which the intensity of a weak harmonic is much less than the Poisson noise of a dominant component using a system of absorbers.

5.5. *Systematic absences*

The data in Table 4 demonstrate that Laue data can be used for assignment of systematic absences corresponding to screw axes. There has been little speculation in the prior literature about how this type of analysis could be performed. In the data sets examined here the combination of the F test and stepwise regression correctly identified

the known systematic absences in all cases. In one case the number of harmonics predicted to be present, 12, exceeded the number of masks, 11. Under these conditions the F test cannot be performed and successful assignment of systematic absences appears to be quite sensitive to the scaling of the unit-cell dimensions. Two approaches can be used to minimize the possibility of mis-assignment of systematic absences in future systems. First, as with the energy measurements and the separation of harmonics, assignment of systematic absences will also be favored by an increase in the number of X-ray photons measured. Second, the foil-mask spectrometer system used here is still a first-generation instrument. Improvement of both the foil sets used and the detection system should be able to improve its performance substantially. Finally, in cases where a large number of harmonics may be present, there is a statistical multiple comparisons problem which may influence the outcome of the separation procedure. In cases which are statistically marginal, initial refinements using a space group of lower symmetry may be advisable to provide additional support for the procedures described here.

6. Conclusions

The use of energy-resolved measurements for the determination of unit cells, separation of harmonics and assignment of systematic absences has been demonstrated. The tolerances required for the measurement of energy are relatively loose; in simulations as much as 3% random error in energy still resulted in satisfactory measurements of the unit cell. When used with a foil-mask spectrometer, all aspects of the method improve with the intensity of the measured X-rays. The method complements methods previously described in the literature and is of similar quality.

Copies of the programs *ERLAI*, *EMATCH*, *EINDEX*, *ESIMUL*, *ESEP* and *EAN* may be obtained through arrangements with the authors; contact qhanley@mpc186.mpibpc.gwdg.de.

The authors wish to thank Dr Michael Bruck for the loan of the crystals of $C_{19}H_{28}O_2$, $MoOS_4N_4C_{28}H_{40}$ and $C_{19}H_{31}MoBN_6O_3$ from the Molecular Structure Laboratory crystal archives, Dr Michael M. Carducci for the donation of the $MoOCl_4PC_{24}H_{20}$ complex, and Dr William Montfort and Dr Sue Roberts for the use of the FR-571 rotating-anode generator and CAD-4. Thanks are also due to CID Technologies for use of the CID camera system, and Thermo-Jarrell-Ash Corporation for monetary support to the Denton group laboratories.

References

Amoros, J. L., Buerger, M. J. & Canut de Amoros, M. (1975). *The Laue Method*. New York: Academic Press.

Bartunik, H. D., Bartsch, H. H. & Qichen, H. (1992). *Acta Cryst.* A**48**, 180–188.

Bragg, W. H. & Bragg, W. L. (1924). *X-rays and Crystal Structure*, 4th ed., pp. 281–283. London: G. Bell.

Bruck, M. A. (1996). Personal communication.

Bruck, M. A. (1997). Personal communication.

Campbell, J. W., Clifton, I. J., Harding, M. M. & Hao, Q. (1995). *J. Appl. Cryst.* **28**, 635–640.

Campbell, J. W. & Hao, Q. (1993). *Acta Cryst.* A**49**, 889–892.

Carr, P. D., Cruickshank, D. W. J. & Harding, M. M. (1992). *J. Appl. Cryst.* **25**, 294–308.

Carr, P. D., Dodd, I. M. & Harding, M. M. (1993). *J. Appl. Cryst.* **26**, 384–387.

Clegg, W. (1984). *J. Appl. Cryst.* **17**, 334–336.

Cruickshank, D. W. J., Helliwell, J. R. & Moffat, K. (1987). *Acta Cryst.* A**43**, 656–674.

Davey, W. P. (1934). *A Study of Crystal Structure and Its Applications*, ch. 3. New York: McGraw-Hill.

Donnay, J. D. H. & Ondik, H. M. (1972). *Crystal Data Determinative Tables*, Vol. II, *Inorganic Compounds*, 3rd ed. Washington, DC: National Bureau of Standards.

Duke, E. M. H., Hadfield, A., Walters, S., Wakatsuki, S., Bryan, R. K. & Johnson, L. N. (1992). *Philos. Trans. R. Soc. London Ser. A*, **340**, 245–261.

Duisenberg, A. J. M. (1992). *J. Appl. Cryst.* **25**, 92–96.

Embree, P. M. & Kimble, B. (1991). *C Language Algorithms for Digital Signal Processing*. New Jersey: Prentice Hall.

Hamilton, W. C. (1965). *Acta Cryst.* **18**, 502–510.

Hanley, Q. S., Dunphy, D. R. & Denton, M. B. (1996). *J. Synchrotron Rad.* **3**, 101–111.

Hanley, Q. S., True, J. B. & Denton, M. B. (1995). *J. Synchrotron Rad.* **2**, 215–228.

Hao, Q., Campbell, J. W., Harding, M. M. & Helliwell, J. R. (1993). *Acta Cryst.* A**49**, 528–531.

Hao, Q., Harding, M. M. & Campbell, J. W. (1995). *J. Synchrotron Rad.* **2**, 27–30.

Helliwell, J. R. (1991). *Nucl. Instrum. Methods*, A**308**, 260–266.

Helliwell, J. R., Habash, J., Cruickshank, D. W. J., Harding, M. M., Greenhough, T. J., Campbell, J. W., Clifton, I. J., Elder, M., Machin, P. A., Papiz, M. Z. & Zurek, S. (1989). *J. Appl. Cryst.* **22**, 483–497.

Kariuki, B. M. & Harding, M. M. (1995). *J. Synchrotron Rad.* **2**, 185–189.

Ravelli, R. B. G., Hezemans, A. M. F., Krabbendam, H. & Kroon, J. (1996). *J. Appl. Cryst.* **29**, 270–278.

Scheaffer, R. L. & McClave, J. T. (1982). *Statistics for Engineers*, ch. 9. Boston: Duxbury Press.

Vetterling, W. T., Teukolsky, S. A., Press, W. H. & Flannery, B. P. (1988). *Numerical Recipes (C)*. Cambridge University Press.

Xiao, Z., Bruck, M., Doyle, C., Enemark, J. H., Grittini, C., Gable, R. W., Wedd, A. G. & Young, C. (1995). *Inorg. Chem.* **34**, 5950–5962.